Passive Discrete Variable Stiffness Joint (pDVSJ-II): Modeling, Design, Characterization and Testing Towards Passive Haptic Interface

Mohammad I. Awad[1]
Khalifa University Center for Autonomous Robotic Systems (KUCARS), Khalifa University of Science and Technology, Abu Dhabi, UAE
Abu Dhabi Campus. PO Box 127788, Abu Dhabi, UAE
mohammad.awad@ku.ac.ae
ASME Membership: ***Student Member*** (000100639263)

Irfan Hussain
Khalifa University Center for Autonomous Robotic Systems (KUCARS), Khalifa University of Science and Technology, Abu Dhabi, UAE
Abu Dhabi Campus. PO Box 127788, Abu Dhabi, UAE
irfan.hussain@ku.ac.ae
ASME Membership (if applicable)

Dongming Gan[1]
Khalifa University Center for Autonomous Robotic Systems (KUCARS), Khalifa University of Science and Technology, Abu Dhabi, UAE
Abu Dhabi Campus. PO Box 127788, Abu Dhabi, UAE
dongming.gan@ku.ac.ae
ASME Membership (if applicable)

Ali Az-zu'bi
Department of Mechanical Engineering, Khalifa University of Science and Technology, Abu Dhabi, UAE
Abu Dhabi Campus. PO Box 127788, Abu Dhabi, UAE
ali.azzubi@ku.ac.ae
ASME Membership (if applicable)

[1] Corresponding authors information: Mohammad I. Awad (mohammad.awad@ku.ac.ae) and Dongming Gan (dongming.gan@ku.ac.ae) .

Cesare Stefanini
Department of Biomedical Engineering, Khalifa University of Science and Technology, Abu Dhabi, UAE
Abu Dhabi Campus. PO Box 127788, Abu Dhabi, UAE
cesare.stefanini@ku.ac.ae
ASME Membership (if applicable)

Kinda Khalaf
Department of Biomedical Engineering, Khalifa University of Science and Technology, Abu Dhabi, UAE
Abu Dhabi Campus. PO Box 127788, Abu Dhabi, UAE
kinda.khalaf@ku.ac.ae
ASME Membership (if applicable)

Yahya Zweiri
Khalifa University Center for Autonomous Robotic Systems (KUCARS), Khalifa University of Science and Technology, Abu Dhabi, UAE
Abu Dhabi Campus. PO Box 127788, Abu Dhabi, UAE
Faculty of Science, Engineering and Computing, Kingston University London, London SW15 3DW, UK;
y.zweiri@kingston.ac.uk
ASME Membership (if applicable)

Tarek Taha
Khalifa University Center for Autonomous Robotic Systems (KUCARS), Khalifa University of Science and Technology, Abu Dhabi, UAE
Abu Dhabi Campus. PO Box 127788, Abu Dhabi, UAE
tarek.taha@ku.ac.ae
ASME Membership (if applicable)

Jorge Dias
Khalifa University Center for Autonomous Robotic Systems (KUCARS), Khalifa University of Science and Technology, Abu Dhabi, UAE
Abu Dhabi Campus. PO Box 127788, Abu Dhabi, UAE
Systems and Robotics and the Faculty of Science and Technology, University of Coimbra, Coimbra, Portugal
jorge.dias@ku.ac.ae
ASME Membership (if applicable)

Lakmal Seneviratne
Khalifa University Center for Autonomous Robotic Systems (KUCARS), Khalifa University of Science and Technology, Abu Dhabi, UAE
Abu Dhabi Campus. PO Box 127788, Abu Dhabi, UAE
lakmal.seneviratne@ku.ac.ae

ABSTRACT

In this paper, the modeling, design and characterization of the passive Discrete Variable Stiffness Joint (pDVSJ-II) are presented. The pDVSJ-II is an extended proof of concept of a passive revolute joint with discretely controlled variable stiffness. The key motivation behind this design is the need for instantaneous switching between stiffness levels when applied for remote exploration applications where stiffness mapping is required, in addition for the need of low-energy-consumption. The novelty of this work lies in the topology used to alter the stiffness of the variable stiffness joint. Altering the stiffness is achieved by selecting the effective length of an elastic cord with hook's springs. This is realized through the novel design of the Cord Grounding Unit (CGU), which is responsible for creating a new grounding point, thus changing the effective length and the involved springs. The main features of CGU are the fast response and the low-energy consumption. Two different levels of stiffness (low, high) can be discretely selected beside the zero stiffness. The proposed physical-based model matched the experimental results of the pDVSJ-II in terms of discrete stiffness variation curves, and the stiffness dependency on the behavior of the springs. Two psychophysiological tests were conducted to validate the capabilities to simulate different levels of stiffness on human user and the results showed high relative accuracy. Furthermore, a qualitative experiment in a teleoperation scenario is presented as a case study to demonstrate the effectiveness of the proposed haptic interface.

1. INTRODUCTION

Conveying information from a remote or virtual environment through haptic interfaces has been an attractive research topic in the last few decades. Haptic Interfaces are typically capable of delivering information to the operator through touch, force or torque [1]. Haptic interfaces are currently applied in several applications and many fields

such as tele-navigation [2-5], tele-rehabilitation [6, 7], tele-surgery [8. 9] as well as micro-manipulation [10, 11].

Classifying haptic interfaces was done based on their haptic stimuli actuation systems which could be active, passive or hybrid. Active haptic interfaces are equipped with actuators that can add or dissipate energy from the system such as motors. Active haptic interfaces have been widely presented in literature, some are grounded like the famous PHANTOM [12], and the haptic arm exoskeletons [13]. Some are wearable like the haptic gloves [14, 15]. On the other hand, passive haptic interfaces are devices that incorporate energetically passive actuators in order to remove, store or redirect kinetic energy within the system [16]. Energy dissipative haptic devices are intrinsically safe and stable compared to their active counterparts, but they're unable to restore energy [17]. Lastly, the hybrid haptic devices apply both active and passive actuation in order to gain the safety and stability of passive actuators and the ability to perform energy restitution from the active actuators [17, 18]. Passive and hybrid haptic interfaces incorporate several types of energy dissipative actuators such as electromagnetic dry friction clutches [19], electro-rheological (ER) clutches [20], programmable differential breaks [21], and Eddy Current Breaks [22].

Elastic elements have also been introduced to haptic device's actuation systems. An example is applying the elastic cords for obtaining egocentric haptic feedback through a body-mounted elastic armature (Elastic Arm) [23]. On the same hand, fabric's stiffness was involved in haptic devices such as the Bi-elastic fabric softness display [24]. A grounded passive device for real time stiffness display was introduced in [25]. More recently, haptic interfaces were equipped with serial elastic actuators (SEA) to enhance the

closed loop behavior and reduce the output impedance [26]. The drawbacks of the SEA lie in the non-optimal performance and non-optimal energy efficiency. The optimal performance needs careful tuning of the joint stiffness values [27, 28]. This motivated lots of study and new designs of variable stiffness mechanisms.

An evolution of variable stiffness actuators (VSA) is the antagonistic variable stiffness actuators, where the joint stiffness is varied through the combination of two antagonistic SEAs controlled by two separate motors. Designs which fall into this category include VSA-I [29], VSA-II [30, 31] and the cable based active variable stiffness module presented in [32]. This type lacks energy efficiency as it requires two motors to adjust the stiffness. In order to overcome this problem, several solutions have been proposed such as altering the link length between the pivot and either the elastic element or the output link. Examples of this type include the AwAS [33], AwAS-II [34], CompAct-VSA [35]. On the same hand, an energy-efficient solution can be realized through discretely selecting the stiffness of the VSA by changing the engagement of elastic material discretely using low power electro-adhesive clutches [30].

For haptic applications, variable stiffness mechanisms were used to simulate different levels of stiffness. Examples for this is the pVSJ [28] where wide range of stiffness can be simulated (from 0 to almost 1000 N,m/rad). This will facilitate applying such device in application where the wide ranges of stiffness needs to be simulated (such as alien environment inspection). In [36], the variable stiffness robotic probe for soft tissue palpation is presented. Altering the stiffness in the probe will enhance the accuracy of detecting hard nodules in soft tissue during abdominal palpation diagnosis. In [37], we proposed the concept of force rendering in haptics through stiffness tuning of the passive

compliant joints for teleoperations of robot interactions with environment in virtual reality or remote scenarios (see figure 1.). In this work, a new version with improved stiffness levels is developed and psychophysical experiments are conducted for haptics perception testing. The proposed system has the potential to be light-weight, portable and low-energy-consumption as a passive system.

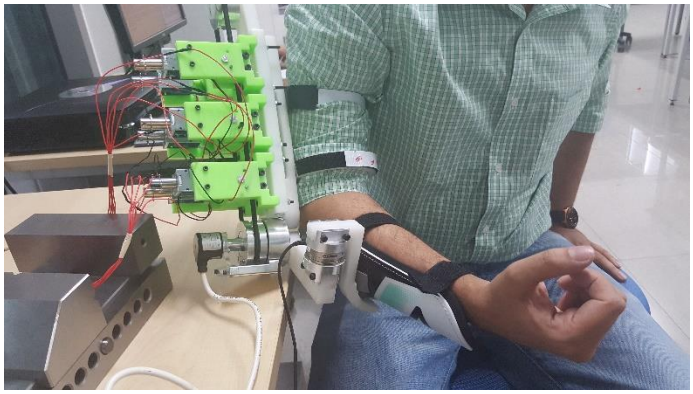

Figure 1: pDVSJ mounted on an elbow exoskeleton [37]

In this paper, a new passive variable stiffness joint is presented. This joint is designated to be used in remote exploration applications where stiffness mapping is required. The proof of concept shows the ability of the joint of switching between levels of stiffness in very short time and minimized energy consumption. The concept and the mechanical design are presented in section 2. The system's modeling, implementation and characterization are presented in section 3. In section 4, psychophysical experiments are conducted, and the results of passive haptics perception are discussed. In section 5, an experiment that demonstrates an example for applying pDVSJ-II as passive haptic interface in a remote palpation scenario is presented. In section 6, a comparison between pDVSJ-II and other variable stiffness mechanisms is illustrated. In section 7, the limitation of the system is being discussed. Finally, in section 8 the conclusions and the intended future work are presented.

2. CONCEPT & MECHANICAL DESIGN

2.1. Design objectives for passive haptics with energy storage components

The interaction with a remote/virtual elastic elements (as shown in fig. 2) starts by compressing/stretching the elastic element (fig. 2b). In this phase (energy storing phase), the generated force/torque is in the opposite direction of motion. When the elastic element is released (energy releasing phase), the force/torque generated by the release of the stored energy is in the same direction of motion (fig. 2c). Passive haptic interfaces with energy dissipative components are only capable to generate forces/torques against the direction of motion. Hence, they're only able to simulate the energy storing phase of the interaction with elastic elements [17]. Therefore, to overcome this limitation without sacrificing the passiveness of the haptic interface, the incorporation of elastic elements (Energy storage elements) will facilitate for the passive haptic interface to fully simulate the interaction with elastic elements.

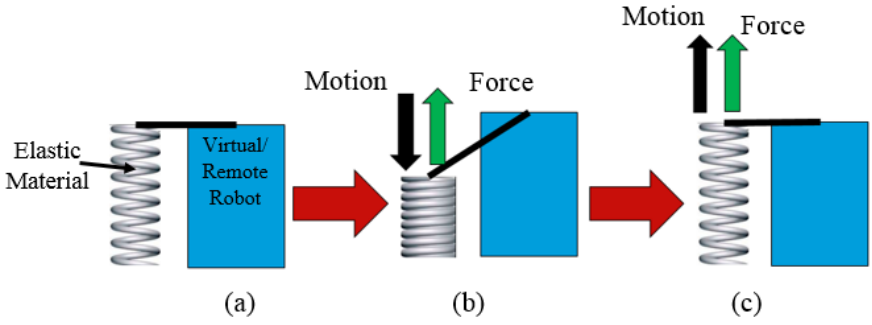

Figure 2: Interaction with elastic remote/virtual component (a) description (b) the interaction when pressing on the elastic component, (c) the interaction when releasing the elastic material

The realization of stiffness mapping of remote (or virtual) environment depends on several design requirements. A haptic interface for this purpose should bare many features such as (1) maintaining transparency (zero stiffness) while no virtual feature is being touched, (2) the transition between one level of stiffness and the other should be instantaneous to insure better mapping quality, (3) the stiffness engagement should occur at any degree of joint deflection and (4) low energy consumption. These features were the motivation drive to design both passive Discrete Variable Stiffness Joint (pDVSJ) and its extension (pDVSJ-II).

2.2. pDVSJ-II Concept and Functionality

The concept of pDVSJ-II is extended from pDVSJ. In pDVSJ [37], the stiffness of the joint is altered instantaneously by discretely selecting the effective length of an elastic cord, while in pDVSJ-II the stiffness is altered through selecting the involved extension spring. The basic concept is shown in (Fig. 3). In the pDVSJ (Fig 3a), an elastic rubber cord with a total length of (Ltot) is grounded from one side and an output force (F) on the other side is generated subjected to an elongation (Δx). It is well known that the stiffness of an elastic cord is inversely related with its length. Thus by engaging different length of the elastic cord in the system, the effective stiffness can be varied. A new grounding point (G) is created by clutching the cord at that particular point creating instantaneously a new active length (Lj). Before the engagement, the output force is $F = \Delta x * k1$, and it is $F = \Delta x * k2$ for the same elongation after the engagement with the effective length Lj.

The main driver to develop the pDVSJ-II is that the available elastic cord used in [37] could not provide the noticeable difference in its stiffness levels for human

perception. Therefore, the elastic cord is replaced with a High Stiffness Cord with Hook's springs fitted on it. This would facilitate more noticeable difference in the stiffness levels for the users when they use the device.

Elaborating on the extended concept, two extension springs are connected in series with each other through a high stiffness cord as in (Fig. 3b). The cord is grounded from one side and an output force (F) on the other side is generated subjected to an elongation (Δx). Assuming that the stiffness of the cord is too high compared to the springs stiffness, the stiffness of the system will include the two springs in series Ksys = (k1k2/(k1+k2). The stiffness can be altered by creating a new grounding point (G). In this case, only one spring is involved and the system's stiffness becomes (Ksys = k2). Applying this approach in altering the stiffness of the elastic material in variable stiffness joints is believed by the authors to be novel.

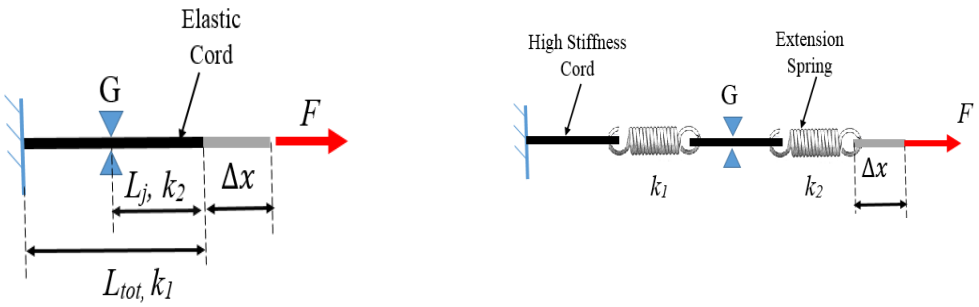

(a) pDVSJ (b) pDVSJ-II

Figure 3: Basic Concepts of (a) the pDVSJ and (b) the pDVSJ-II

The pDVSJ-II (shown in Fig. 4) consists of a high stiffness cord with a set of four extension springs attached to the cord. The cord is looped and mounted on two pulleys. The cord is fixed on two symmetrical points (Points A, A*) on the joint pulley while winds

around the driven pulley. In order to create new grounding point, a novel unidirectional selective-self-locking mechanism is used, these mechanisms are called Cord Grounding Units (CGU). A set of four Cord Grounding Units (CGU) allow the cord to move freely while not activated, taking the assumption that the springs and the cord will move as a rigid body in the case where there is no restriction in the cord's motion, as well as the negligible levels of friction in the pulley. In this case, the transparency level (zero stiffness value) is achieved. A CGU will prevent the cord from moving in one direction if activated to create a grounding point, the position of the grounding point will define the involved springs. The CGUs labeled (L, H) are assigned to prevent the cord of moving in the direction when the output link is moving Counter Clockwise (CCW). CGU L will engage both springs to provide low stiffness while CGU H involves only one spring to have the high stiffness. Similarly, the CGUs labeled (L*, H*) are for Clockwise (CW) motion. The (*) refers for any entity or variable that is related for the CW motion.

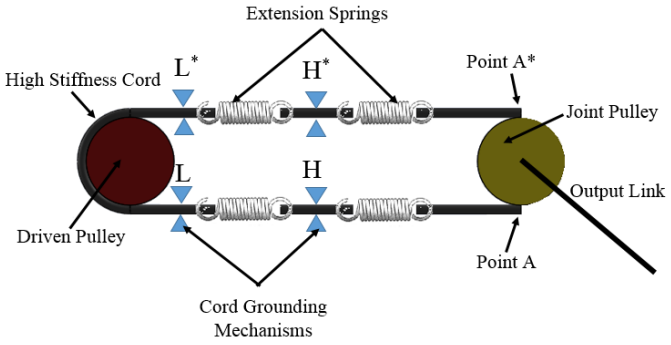

Figure 4. Functionality of the pDVSJ-II

2.3. Cord Grounding Unit

A key component of the proposed system is the Cord Grounding Unit (CGU) which is a selective-self-locking mechanism aimed for creating the grounding point through clutching the motion of the moving cord on a defined position in order to alter the stiffness of the system. CGU can be controlled selectively whenever locking process is required. Locking process requires (1) a control pulse and (2) the motion of the cord in the designated clutching direction. However, unlocking is a passive process. It requires only the motion of the cord in the opposite direction of the clutching ones.

In a system with multiple CGUs, the locking and the unlocking features would allow stiffness to be altered from low stiffness levels to higher levels of stiffness without the need of unlocking the low-level CGUs. For example, in (Fig.3) if CGU-L was locking the cord, the stiffness level L will be present. If CGU-H was locked during that time, stiffness H will be present even CGU-L is still locked. On the other hand, if CGU-H was locked, the lower levels of stiffness cannot be achieved unless CGU-H is unlocked. Although this feature may seem to be a limitation, it is actually consistent with real-world compliant interactions, for which stiffness typically follows a non-decreasing behavior with respect to the applied compressive force [38].

The CAD model of the CGU is shown in (Fig. 5). The CGU is composed of a frame, a cam-cleat, a linear solenoid actuator, and a leaf spring. The cam-cleat's shaft is mounted on the frame and can rotate freely. Unlike the regular cam-cleat applications, the leaf spring is responsible of retracting the cam-cleat away from the clinging point. The design procedure of the cam-cleat's profile has taken into account the maximum cord diameter with extra clearance to avoid undesirable friction while the CGU is inactive. When the

CGU is activated (see Fig. 6), it is desired that the engagement between the moving cord and the cam-cleat to be with some angular displacement from vertical line from the cam's center of rotation and the cord (Vector R). This displacement with the pulling force (F_t) of the cord are responsible of creating the torque (τ) necessary for the cam cleat to move towards the clinging point.

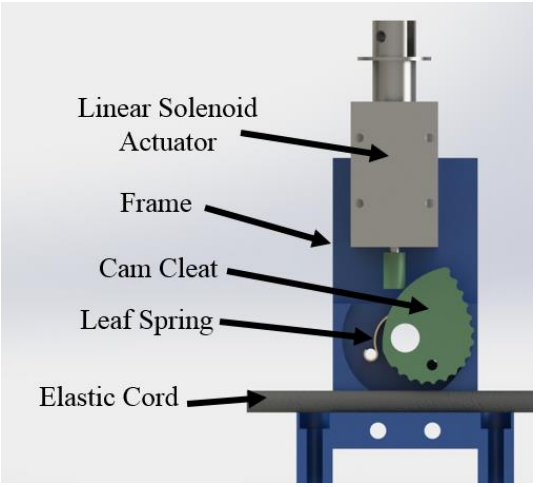

Figure 5: Anatomy of Cord Grounding Unit

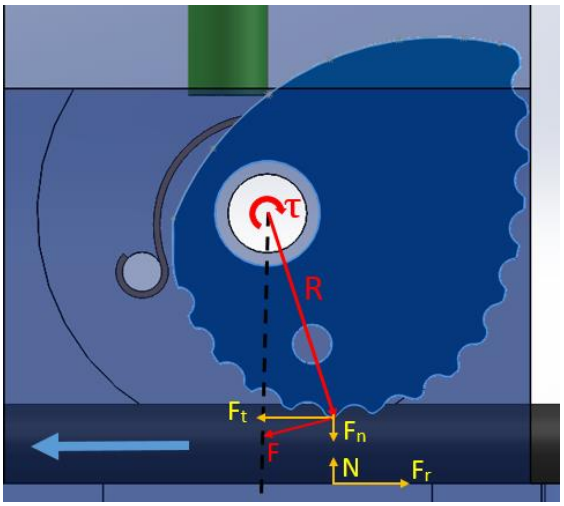

Figure 6: Parameters taken in consideration for the cam-cleat profile design

In order to create a grounding point (blockage in motion), the friction force (Fr) should be maximized. And this can be achieved by increasing the two normal forces on the cord's direction of motion. The first force is the one between cord and the cam cleat (F_n), and the other one between the cord and the frame (N). It's worth to note that (F_n) is normal projection of the force (F), which is created by the radius (R) and torque (τ). Its worthy to mention that the Cord's transversal stiffness also plays an important role in the proposed system, allowing for progressive cam's rotation and increasing clinching when pulling force increases. Cam's profile parameters have therefore been selected taking into account cord type and thickness. Several off-shelf cam-cleats were analyzed and modeled. The cam-cleat used in the proposed design was modeled with a fourth-order-polynomial function which was obtained by the authors as best fit polynomial curve for common off-shelf cam-cleats. The resulting profile function is as follows:

$$R = \alpha_1\theta^4 + \alpha_2\theta^3 + \alpha_3\theta^2 + \alpha_4\theta + \alpha_5 \quad (1)$$

where R, θ, αi are the cam's radius, angular displacement, and regression constants respectively. The regression constants are illustrated in Table I. The gap (R_G) between the cam-cleat and the frame is the difference between the cords diameter (D_c) and cam-cleat's profile (R) (i.e. $R_G = D_c - R$). The gap versus the angular position of the cam-cleat is illustrated in Fig. 7. It can be seen that the gap can allow a cord up to 8 mm diameter (with 0.5 mm clearance) to run through CGU. The gap was virtually eliminated at cam-cleat angular position of 130.4 degrees.

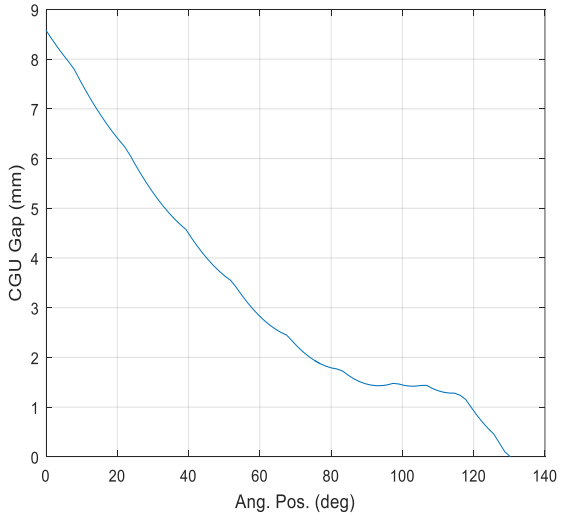

Figure 7: CGU Gap vs cam-cleat angular position

Table 1: Cam-cleat profile constants

Specification	Value
$\boldsymbol{\alpha_1}$	1.17
$\boldsymbol{\alpha_2}$	-5.46
$\boldsymbol{\alpha_3}$	6.09
$\boldsymbol{\alpha_4}$	4.82
$\boldsymbol{\alpha_5}$	10.26

The key feature of the CGU is its low energy-consumption. This can be facilitated through the operating stages of the CGU illustrated in Fig.8. When the joint is running in the transparent mode (zero stiffness) the cord is running freely and the cam cleat is pushed away by the retracting spring (Fig 8a). Whenever altering the stiffness is required, the solenoid is activated to only maintain a low force for short time “touch” between the cam-cleat and moving cord before the cord starts pulling the cam-cleat (Fig. 8b). Afterwards, the cords pulls the cam-cleat towards the locking position without the need of the solenoid’s assistance (Fig. 8c). In an ideal scenario, where the cord’s motion is not

affected significantly by its elasticity along its length, the ON-time of the linear solenoid actuator will be a short period depending on the time needed to form a grounding point.

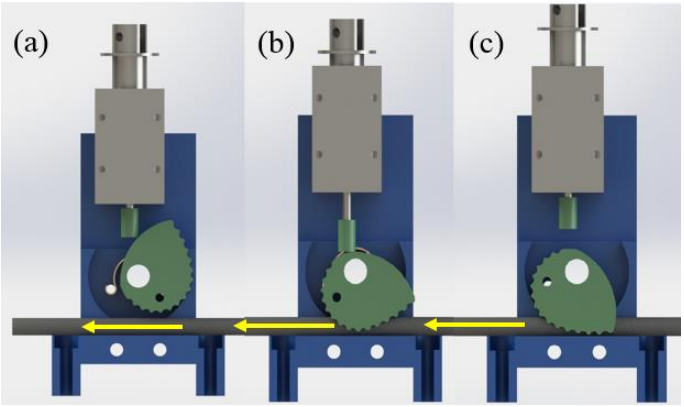

Figure 8: Cord Grounding Unit Operating Stages

The change in stiffness will take place at the instant the grounding point is created. The amount of time needed to create a grounding point (Response Time) is directly related to the cord's axial velocity (V) and the maximum compressibility (γmax) of the cord. (Defined as the ratio of the maximum reduction in the cross-sectional diameter of the cord with respect the free cord's diameter) The response time (T_{res}) can be determined as follows:

$$R_G(\theta_{GP}) = D_c(1 - \gamma_{max}) \qquad \gamma_{max} \in (0,1) \tag{2}$$

$$T_{res} = \Delta t = \int_{\theta_0}^{\theta_{GP}} \frac{R(\theta)}{V} d\theta \tag{3}$$

Where $R_G(\theta_{GP})$ is the CGU gap value when the grounding point is generated, and θ_{GP} is the angular position of the cam cleat when the grounding point is generated. For

example, if the maximum compressibility of an 8 mm diameter cord is 45%, the grounding point will be generated when the CGU gap is approximately 4.5 mm. Using Fig 6, the angular position of the cam-cleat where the grounding point is created (θ_G) is approximately 40 degrees. For a 50 mm/s cord's axial speed, the response time is 174 ms. In Fig. 9, the response time vs. cord axial velocity is illustrated for different values of γ_{max}.

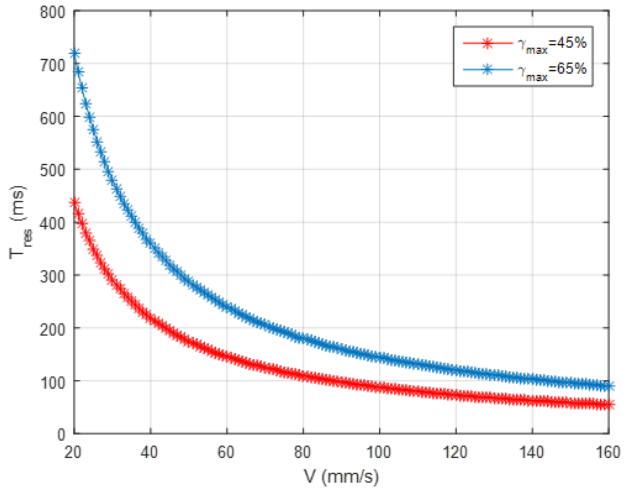

Figure 9: Response time vs cord's axial velocity for different values of γ_{max}

The minimum electrical energy (E_{min}) required to change the stiffness can be determined using the following equation:

$$E_{min} = Q_{sol}(T_{res} + T_{sol}) \quad (4)$$

where Q_{sol}, T_{sol} is the electrical power consumption and the response time for the solenoid respectively. The selected solenoid operates at 40.8 W and has a response time of 40 ms.. For a cord with 45% compressibility, the simulation shows that the

minimum energy required to alter the stiffness varies from 4.01 – 37.3 J. (For a range of cord speed of 10 – 150 mm/s)

3. SYSTEM MODELLING & CHARACTERIZATION

The elastic elements embedded in the pDVSJ-II are the tension springs and the high stiffness polymer cable In subsections 3.1 and 3.2., the stiffness analysis of each element is illustrated. Then the system's stiffness model and its experimental validation are presented in subsections 3.3 and 3.4 respectively. Finally the estimation of the system's dynamic parameters is illustrated in subsection 3.5.

3.1. Tension Springs

In the pDVSJ-II, four tension springs are used. This type of springs is known to obey hook's law in their "safe-travel" region, which requires determining the initial pretension force point and the non-linear behavior starting point. A sample of the fabricated springs was tested on Tensile Test Machine (Instron 5969) in order to empirically determine their safe travel regions. The results (Fig. 10) shows that the initial pretension force is approximately 19.6 N, where the spring starts to follows hook's law with a stiffness of 5.33 N/mm. The spring's stiffness stays constant till elongation exceeds 12 mm which yields a safe travel region around 11.5 mm. It must be noted here that it is desirable from the designer's prospective to keep the springs in their safe travel region to simplify the modeling and avoiding the plastic deformation of the springs which would affect their functionality permanently. Hence, pretension is added while mounting the HSP cord on

the pulleys. In order to prevent reaching the non-linear region behavior of the springs, the maximum deflection of the joint is limited to the safe travel range of the springs.

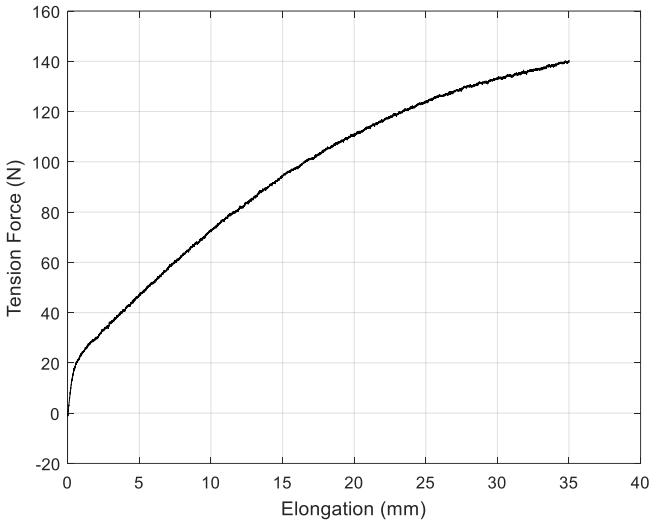

Figure 10: Tension Force vs Elongation for tension Hook Spring

Taking in the assumption that the springs are identical and connected in series, their stiffness can be represented as follows:

$$K_{sj} = \frac{K_s}{j} \tag{5}$$

where Ks, j are the Linear spring's constant, and the number of involved springs respectively.

3.2. High Stiffness Polymer (HSP) Cord

The other elastic component included in pDVSJ-II is the High Stiffness Polymer (HSP) cord. Polymers elastic behavior does not follow Hook's Law due to entropy [39]. Stiffness of polymers depends on several factors such as (1) Ambient Temperature, and (2) the polymer's cross link density [39]. Since adding these factors results in further

complexity to the system's model, it is worthwhile to study the operating regions of the elastic cord and select a preferred region that simplifies the modeling process.

Two samples from the polymer cord with initial lengths, (51mm, 77mm,) were tested using a Tensile Test Machine (Instron 5969) . The force vs. strain graph shows that cord behaves nonlinearly in the toe region (strain: 0 to 0.02); then becomes linear in the second region (strain: 0.02 to 0.25); and finally reverts to nonlinear behavior with a higher order of magnitude in the third region (strain: above 0.25). Therefore, the desired operating region of this cord is chosen to be the linear region, and hence a minimum pretension level of 0.02 strain should be set.

As depicted in Fig. 11, the stiffness of the HSP cord (K_{Li}) in the linear region can be determined from the known length at the clinging time (L_{i0}) of the cord :

$$K_{Li} = \frac{\mathrm{K}_{HS}}{\mathrm{L_{i0}}} \tag{6}$$

where KHS is the rate of change in load force with respect to the obtained strain (KHS =4771.1 N) from Fig.11.

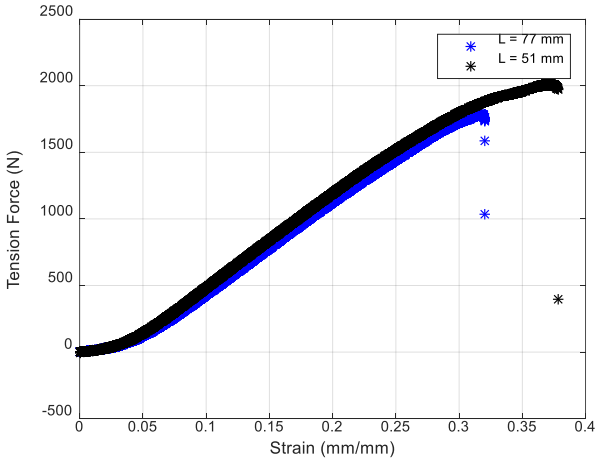

Figure 11: Tension Force vs Strain for HS Polymer Cords

3.3. Stiffness Modeling of pDVSJ-II

In pDVSJ-II, the stiffness is altered through selecting the number of involved springs. Fig. 12 shows that the number of involved springs can be selected through activating the desired CGU. In (Fig. 12a), the CGU (H*) is activated (red), therefore, one spring is involved with two segments of HS polymer cord (segments 1 and 2). In (Fig. 12b), the CGU (L*) is activated, therefore, two springs are involved with three segments of HSP cord (1, 2, and 3).

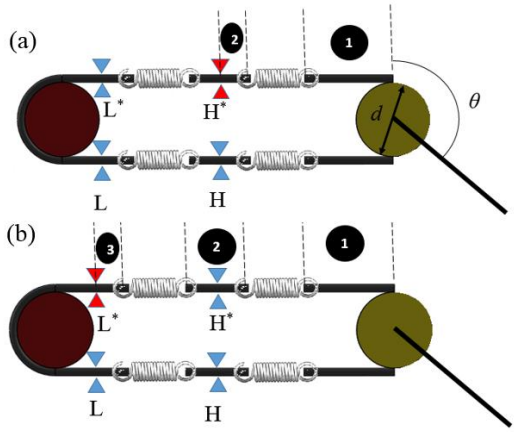

Figure 12. Model of the pDVSJ

A stiffness model of the joint is presented in this section. It is assumed that the joint will operate in room temperature, and the HSP cord's cross link density will not be effected by the cross-sectional compression applied from the CGU. It is also assumed that the cord with the active length and the cord with the remaining length behave independently from each other.

Stiffness of the pDVSJ-II is the sum of the stiffness of the selected segments in series. As the Tension Hook Springs are identical, their stiffness is considered constant at any position when the designated CGU is selected. For the HSP cord segments, if the length of the segment is not affected by creating a new grounding point, the stiffness of that segment is also constant. In the case of CGU H is activated, segments 1 have predetermined stiffness values, while the segment 2 may have different levels of stiffness depends on its involved length after grounding. The involved length depends on the pDVSJ-II joint's position. The same applies for segment 3 when CGU-L is activated. This can be described as follows:

$$L_{20} = L_2(\theta_0) + r(\theta_a - \theta_0) \qquad \text{if CGU H=active} \tag{7}$$

$$L_{30} = L_3(\theta_0) + r(\theta_a - \theta_0) \qquad \text{if CGU-L=active} \tag{8}$$

where L_{20}, L_{30}, θ_a, θ_0 are the involved length of segment 2 (Fig.12a), involved length of segment 3 (Fig 12b), angular position of the pDVSJ-II when the designated CGU was activated (will be denoted as the activation position hereafter), and the initial position of

the pDVSJ-II respectively. It must be highlighted that in case of CGU-L is active, L3 will be at its maximum length.

As all elastic components are connected in series, their total stiffness (K_{tot}) and the output torque (τ_{out}) equation can be written as following:

$$j = \begin{cases} 1 & if \ \text{CGU} - \text{H is active} \\ 2 & if \ \text{CGU} - \text{L is active} \end{cases} \tag{9}$$

$$n = \begin{cases} 2 & if \ \text{CGU} - \text{H is active} \\ 3 & if \ \text{CGU} - \text{L is active} \end{cases} \tag{10}$$

$$K_{tot} = \left(\sum_{i=1}^{n} ((K_{Li})^{-1}) + \left(K_{sj}\right)^{-1} \right)^{-1} \tag{11}$$

$$\tau_{out} = \frac{d}{2}(K_{tot}\Delta x) + \ \tau_p \tag{12}$$

$$\Delta x = \frac{d}{2}\Delta\theta \tag{13}$$

where $j, n, x, \ d, \theta, \tau_p$ are number of involved springs, the number of involved HSP cord segments, linear elongation, pulley's diameter, joint angular displacement, and pretension torque respectively. Substituting (13) into (12), then deriving with respect of the joint's angular position (θ). Accordingly, the joint's stiffness (K_θ) can be written as following:

$$K_\theta = \frac{\partial \tau_{out}}{\partial \theta} = \left(\frac{d}{2}\right)^2 K_{tot} \tag{14}$$

From (11 and 14), it is shown that the joint's stiffness can be discretely chosen by selecting the involved springs and HSP cord segments. It can also be concluded that for

each activation position, two levels of stiffness can be achieved through activating either CGUs. Through the joint space (0, π/2), the effect of different activation positions on the value of total stiffness Ktot in (11) can be seen in Fig. 13. The maximum change in the total stiffness with different activation positions along the joint space is 6.6% and 3.35% for the activation of CGU-H and CGU-L respectively.

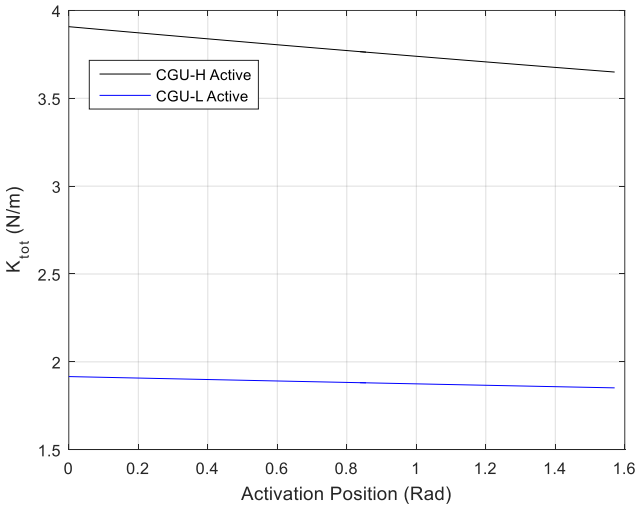

Figure 13. The variation in the values of the Total Stiffness in (8) vs the activation position. The stiffness values are slightly effected through the span of activation positions

3.4. Physical Implementation and Model Validation Experiments

The structure of pDVSJ-II consists of one Aluminum base (back arm) link and a Teflon link (forearm). The back arm is (480 mm) long and consists of a link, a base for the CGUs and the driven pulleys. The forearm link is (125 mm). The pulleys (driver and driven) are made of Aluminum Alloy with (55 mm) diameter. The cam-cleats and the frames of the four Cord Grounding Units (CGU) were 3D printed and are made of Acrylonitrile Butadiene Styrene (ABS) Light Plastic. The CGUs were mounted along the base on the back arm so that the effective lengths will be LH=180 mm, and LL= 380 mm. The Linear Solenoid

Actuators operate at 24 VDC and draw a current of 1.7 Amperes each while active. The system's design parameters are shown in Table 2.

Table 2: pDVSJ-II Design Parameters & Specifications

Specification	Value	Unit
Linear Spring's Stiffness	5.686	N/mm
TELEXOS-I Back Arm Length	0.48	m
TELEXOS-I Forearm Link Length	0.125	m
Pulley's Diameter	0.055	m
HSP Cord Rate of Change of Force to Strain	6298.1	N

The sensory system of pDVSJ-II consists of a force/torque sensor (ATI Mini 40) mounted on the forearm, and a quadrature rotary encoder (RS-260-3768) mounted on the driver pulley. A National Instrument DAQ (NI-USB-6343) and the National Instrument LabVIEW® were used for real time control and data acquisition. The test for characterization was performed on a horizontal vice (fig. 14) to eliminate the gravitational potential energy effect.

To verify the stiffness model, several experiments were conducted. By selecting to activate the desired CGU, the user will apply the external torque through a block held by their hand in order to deflect the joint from the home position (zero degrees) to around 90 degrees. The deflection was measured by the optical encoder and the external torque was measured by the force/torque sensor.

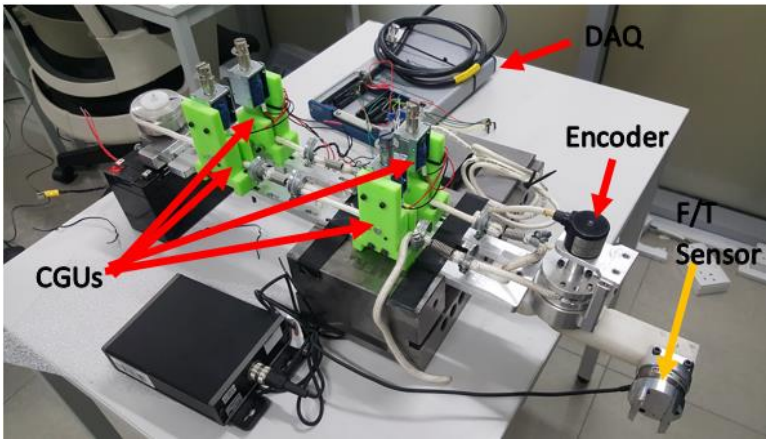

Figure 14. Characterization experiment of pDVSJ-II

In (Fig. 15), the experimental results (black circles) have validated the presented theoretical model (red lines) for all the two stiffness levels. It's worth to mention the hysteresis behavior in the experimental behavior is mainly due to the HSP cord material behavior. This is due to the fact that polymers experience energy dissipation during loading and unloading due to the polymer's material internal friction [40].

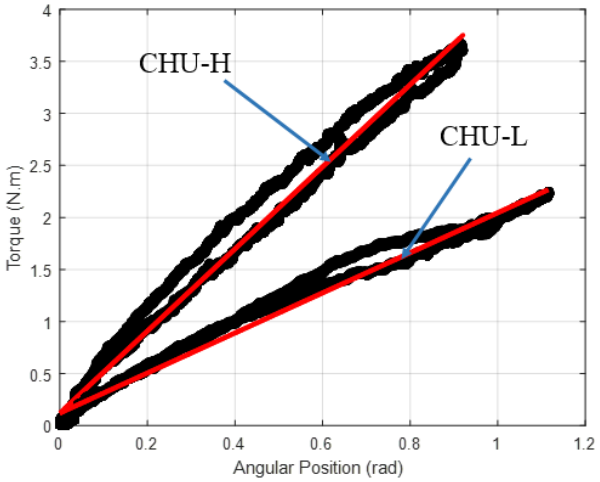

Figure 15: Joint's Torque versus Deflection: Theoretical results (Red Lines), experimental results (black circles)

Regarding the system's power consumption, it is noted that the solenoid's ON-time under a joint average angular speed of (5.2 degrees/s) is (1 second). its noteworthy here that the elasticity of the cord's material has significantly affected behavior of the cord's motion flow. A change in the position of the joint's link will immediately change the position of the cord that is near to the joint pulley resulting a stretch in that part of the cord. While the other part far away from the pulley is still un-stretched and stationary. Then the load is distributed along the cord yielding the lag in motion of the end of the cord compared to its beginning. Thus, the longer the cord length, the bigger the lag in motion appears. This explains the longer ON-Time duration for the solenoids of CGU-L (2 seconds) compared to CGU-H. The system's power, and physical specifications are shown in Table 3.

Table 3: System's Power and Physical Specifications

Specification	Value	Unit
Operating Voltage	24	VDC
Operating Current	1.7	A
Power Consumption for Single CGU	40.8	W
Linear Solenoid Actuator response time	40	ms
Single CGU Mass	225	g
Single Linear Solenoid Actuator	150	g

3.5. Dynamic Model

pDVSJ-II is a passive single degree-of-freedom rotary joint that can alter its stiffness level without affecting the passivity of the output. The output link's moment of inertia and the system's damping coefficient are designated to have small values. The dynamic model can be represented as simple inertia-damping-spring model as follows

$$I\ddot{\theta} + B\dot{\theta} + K\theta = \tau_h \quad (15)$$

Where I, B, K, τh, θ are the moment of inertia, damping coefficient, stiffness, input (hand) torque, and angular deflection respectively. The stiffness coefficient can be calculated through the stiffness model presented in the stiffness model section. The moment of inertia can be theoretically estimated through Computer-Aided-Design software (SolidWorks 2013).

In order to estimate the damping coefficient, pDVSJ-II was subjected to a fixed input torque equalized by the spring tension. From this equilibrium state, pDVSJ-II is released and the angular position is recorded. Applying the Nonlinear Least Square Method, all dynamic parameters were estimated empirically. Table 4 illustrates the estimated parameters theoretically and empirically. From the results, it can be concluded that for a system with low speed and acceleration the effect inertia and damping effects will be very low compared to the stiffness coefficient. The bode plot for the system is illustrated in fig. 16. It can be concluded from the figure that the bandwidth of the system is relatively low and can hence be used for some applications, like haptic exploration tasks [41, 42].

Table 4: Dynamics System Coefficients for pDVSJ-II

Parameter	Theoretical Value	Estimated Value	Unit
I	0.00309	0.00319	Kg.m2
B	N/A	0.03189	N.m.s/rad

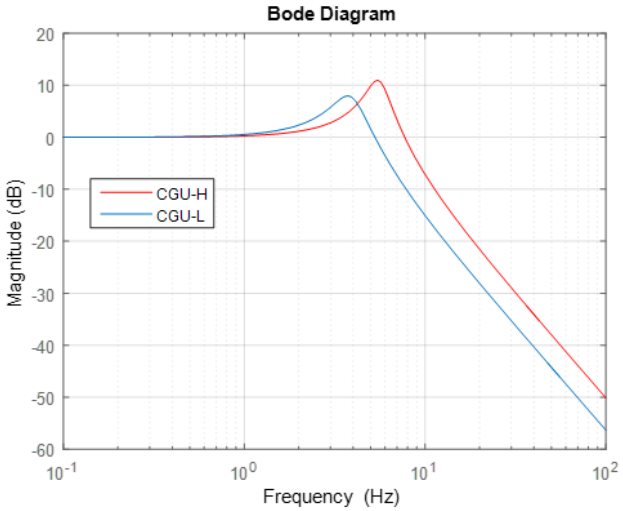

Figure 16. The bode plot of the system for both levels of stiffness (High: red, Low: blue). The bandwidth for the system in high stiffness and low stiffness are 8.52 Hz, 5.88 Hz, respectively

4. PSYCHOPHYSICAL EXPERIMENTS

Upon approval of the ethics committee at Healthpoint Hospital in Abu Dhabi, two series of psychophysical experiments were performed on human subjects. The experiments aimed to measure the capability of the novel pDVSJ-II joint to display two levels of stiffness that are cognitively sensed (differentiated) by the users. The test procedure is based on [41]. As pDVSJ-II is totally passive, only active-push cognitive tasks were performed, similar to the active-touch cognitive tasks performed in [41]. These tasks consisted of the Relative Cognitive Task and Absolute Cognitive Task, based on literature. In this section, the experimental design and setup, the participant's selection criteria, the detailed procedures of each cognitive task, and the results of the experiments are described.

4.1. Experimental Setup

Two calibrated torsional springs were mounted on a device that mimic's the output link of pDVSJ-II (see fig. 17). The springs are made of Stainless Steel A316 Alloy. The detailed design parameters of the springs are shown in Table 5. Hereinafter, the springs (Spring-H) and (Spring-L) with their devices will be labeled as SH and SL respectively. The stiffness values of the springs were selected to be approximately equal to the stiffness levels rendered by the pDVSJ-II. This facilitates the matching process between the rendered pDVSJ-II stiffness and the mimic devices to the participants.

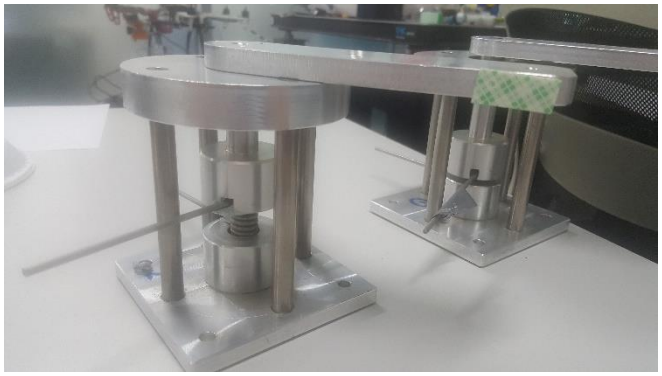

Figure 17: Stiffness Mimic Devices with Calibrated Springs

The tips of the output link of SH, SL and pDVSJ-II were covered with 1 mm plastic pads in order to eliminate any confusion in the user perception per to the material softness or temperature.

Table 5: Springs parameters for the Stiffness Mimic Devices

Parameter	Spring H	Spring L	Unit
Torsional Stiffness	69.69	33.23	N.mm/degree
Wire Diameter	3	3	mm
Outer Diameter	14	14	mm
Number of Active Coils	5.25	11	coils
Safe Travel Angel	32	67	degrees

4.2. Participants

For the two tasks, (20) right-handed healthy participants (9 Females, 11 Males, Age: (30.5 ± 3.74) gave their informed consent to participate in the experiment. Exclusion criteria consisted of any upper-body physical limitations, disease or movement dysfunction that may have affected the experimental outcomes. The experimental procedure was approved by the Ethics Committee of the Healthpoint Hospital – Abu Dhabi – United Arab Emirates (Ref. REC006).

4.3. Active Relative Cognitive Task

During this task, the participants were asked to use the tips of their thumbs to probe and sort the two levels of stiffness rendered by pDVSJ-II. They were subjected to 5 sets of stiffness levels. In each set, 2 levels of stiffness were randomly displayed, and the participants needed to rank them from the lower stiffness to the higher stiffness. The participants were seated on a chair, blind-folded and subjected to acoustic white-noise in order to shield any auditory or optic cue, and were granted unlimited time to perform their tasks. They were guided to push the stylus of pDVSJ-II by the thumb of their dominant hand such that the stylus deflected around 30-45 degrees. The results are shown in Table 6, where the perception of the stiffness displayed by pDVSJ-II was

associated with the perception of the real values in a typical confusion matrix. The diagonal of the matrix represents the correct answers.

Table 6: Confusion Matrix of Relative Cognitive Task

	CGU-H	CGU-L	Relative Accuracy (%)
CGU-H	87	13	87
CGU-L	12	88	88

4.4. Active Absolute Cognitive Task

In this task, the participants were guided to use the tips of their thumbs to probe two levels of stiffness as rendered by pDVSJ-II, and then relate them to their physical counterparts displayed on the mimic devices. They were subjected to 5 sets of stiffness levels, where in each set 2 levels of stiffness (pDVSJ-II) were randomly displayed and the participants needed to relate/match the rendered stiffness with its physical counterpart using his left hand. The participants were seated on a chair, blind-folded and subjected to acoustic white-noise shielding any auditory or optic cue. Granted an unlimited time to perform their tasks, the participants were guided to push the stylus of pDVSJ-II by their right thumbs and the stylus of the mimic device by their left thumb such that either stylus deflects around 30-45 degrees (as illustrated in fig. 18). The results are shown in Table 7, where the perception of the stiffness displayed by pDVSJ-II was associated to the perception of the real values in the mimic devices in a confusion matrix. The diagonal of the matrix represents the correct answers. The errors of the absolute cognitive task can be related to the laterality of the participants.

Table 7: Confusion Matrix of Absolute Cognitive Task

	SH	SL	Relative Accuracy (%)
CGU-H	81	19	81
CGU-L	28	72	72

Figure 18: Participant performing the Absolute Cognitive Task

4.5. Results Discussion

Comparing the results of pDVSJ-II with the validated haptic interfaces proposed in [41, 43], The results show that the users have recognized the levels of stiffness rendered by the pDVSJ-II with an average of 87.5% for the Relative Cognitive Task, and 76% for Absolute Cognitive Task. In [41], similar experiments were conducted on the validated haptic interface and the results of the Relative Cognitive Task is 91% and Absolute Cognitive Task is 82%. While in [43], only Relative Cognitive Task is conducted to validate the proposed device and the results are an average of 70%. From this, it can be concluded that pDVSJ-II is verified as haptic interfaces.

5. HUMAN-ROBOT APPLICATION: REMOTE PALPATION USING PASSIVE DISCRETE VARIABLE STIFFNESS JOINT (PDVSJ-II)

Palpation is defined as the application of the fingers with light pressure to the surface of the human body for the purpose of determining the condition of the parts

beneath during physical diagnosis [44]. Palpation with a robotic device, or artificial tactile exploration of soft viscoelastic and nonhomogeneous objects, is an important area of study for various fields including medical, virtual reality or teleoperation applications. In order to demonstrate the effectiveness of pDVSJ-II, a qualitative experiment simulating a palpation teleoperation scenario was conducted. In teleoperation [45], the human and the robot are separated spatially or temporally for remote interactions.

While mainly aiming to demonstrate the effectiveness of the pDVSJ-II for passive haptics applications, the experiment also explores finding an intuitive way to identify any hard abnormalities, such as tumors, in soft tissue palpation from a remote environment. As the device's quality for rendering two levels of stiffness and be recognized by users was tested and confirmed in the psychophysical tasks experiments in section 4, its worthy to mention that this experiment may also provide confirming results for understanding how humans are able to discern the two levels of stiffness rendered by the device.

5.1. Experimental Setup

The proposed teleoperation system was composed of the passive Discrete Variable Stiffness Joint (pDVSJ-II), a 2 arm, 7-DoF per arm Baxter manipulator (Rethink Robotics, MA, US) , and a ATI Delta force/torque sensor (ATI Industrial Automation, NC, USA), opti-track system (Optitrack, Natural Point Inc. OR, USA), two objects with different stiffness. Each object was placed on a specific position on the table in front of the robot. The force/torque sensor was placed under the object to record the force applied by the robotic manipulator right arm on the top of the object (see Fig. 19). The block diagram of the experimental setup is shown in Fig. 20. We used the Optitrack system

(Optitrack, Natural Point Inc. OR, USA) to record the positioning of the robotic manipulator and the movement of the subject's arm. The force/torque sensor, the Optitrack system and robotic manipulator are connected with the computer which is connected with Arduino Uno board using serial communication. On the master side, the Arduino controller is connected with the Relays which activates/deactivates the solenoids of the CGUs which are responsible of selecting the level of stiffness provided by the device.

The experiments were implemented by using a finite state machine (FSM) as shown in Fig. 21. The information from the slave side was collected by the ATI force/torque sensor and the Optitrack motion capture system and fed back to the user on the master side through the pDVSJ-II. The exchange of messages between all the different devices was managed by the Robotic Operating System (ROS) framework, an open-source Robot Operating System [46].

5.2. Participants

Three right-handed participants (2 males, 1 female, average age 30) participated in this qualitative study. None of the participants reported any deficiencies in their visual or haptic perception abilities. The participants were briefed about all the tasks and then signed an informed consent. Headphones were worn by the participants to mask the noise of the Baxter motors. The experiment did not involve the processing of genetic information or personal data (e.g., health, sexual, lifestyle, ethnicity, political opinion, religious or philosophical conviction). The experimental procedure was approved by the

Ethics Committee of the Healthpoint Hospital – Abu Dhabi – United Arab Emirates (Ref. REC006).

Figure. 19: The experimental set up: The Baxter manipulator having the tracking markers at its end effector to register the vertical motion. The haptic interface (pDVSJ-II) has tracking marker at its end effector. The motion of both robot and pDVSJ-II end effector are recorded through Optitrack system. The ATI Delta force sensor is placed under the object to measure the applied force. Arduino Uno along with the 24V relays is used to activate/deactivate the solenoid to alter the stiffness of the device

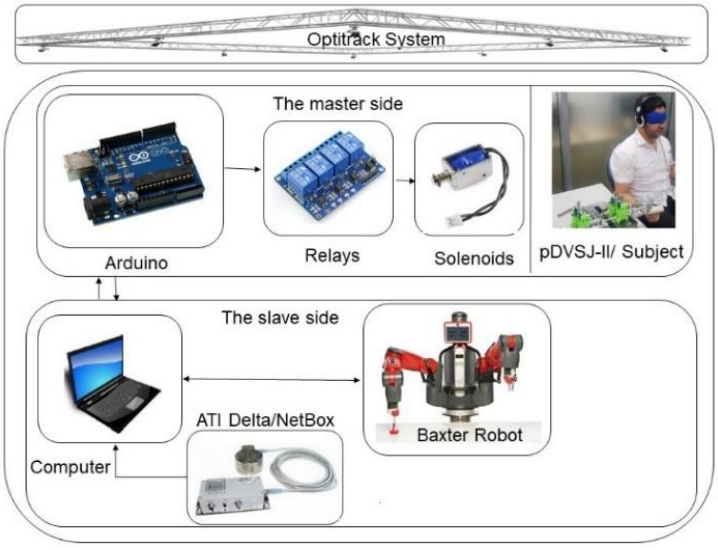

Figure. 20: Block Diagram of experimental setup. The Optitrack system to record the motion at both master and slave side i.e. the position of end effector's of robot and pDVSJ-II device and

communicate with the computer through ROS. On the slave side, the Baxter Robot, ATI Delta along with its NetBox controller are connected with the computer and also use the ROS as communication interface. On master side, the arduino UNO is connected with computer through serial communication which in turns control the relays to activate/deactivate the solenoids to change the stiffness of pDVSJ-II accordingly.

5.3. Methods

The participants were asked to control the robot on the slave side by the end effector of pDVSJ-II using direct visual feedback of the remote environment. All the possible behaviors of the robot are described by the finite-state machine depicted in Fig. 20. The system events "a" and "b" were characterized by a keyboard key while f_c, K_1, and K_2 were automatically generated through the sensors' information. Because of the intuitive control, the finite-state machine is considered simple in terms of input commands. The type of interaction depends on the current state.

The various states as described as follows:

S1 – Stand-by: the pDVSJ-II and the Baxter robotic manipulator are initialized; all the connections between each controller and the computer are established. The linear solenoid actuators are completely open to facilitate the movement of the elastic cord.

S2 – Set home: The robotic arm reaches the starting position.

S3 – Control switched to pDVSJ-II device end effector and now onwards, the robot moves in proportion to the motion of the device's end effector. ($\Delta z = \alpha \Delta\theta$) where ($\Delta z$, $\Delta\theta$) are the displacement in the slave's end-effector, and the angular displacement of the master device (pDVSJ-II). (α) is a constant.

S4 – Contact with object: The connection between the robot and the pDVSJ-II is enabled, i.e., the controller of the solenoid acts according to what happens at the remote site. The subjects are asked to slowly move the robotic manipulator with the help of the

end effector of the pDVSJ-II until the gripper of the manipulator comes in contact with the surface of the object, which is recognized through a force threshold as read by the ATI force sensor.

S5– Stiffness level 1: The first stiffness level of the object is recognized through the force sensor and fed back to the user by activating the corresponding solenoids using the Arduino.

S6– Stiffness level 2: The second stiffness level (i.e. the relatively hard surface) of the object is detected and the higher stiffness stage of the device is activated to simulate the high stiffness to the participant. An experimental trial can be considered accomplished when, all the states are successfully completed (S1 to S6).

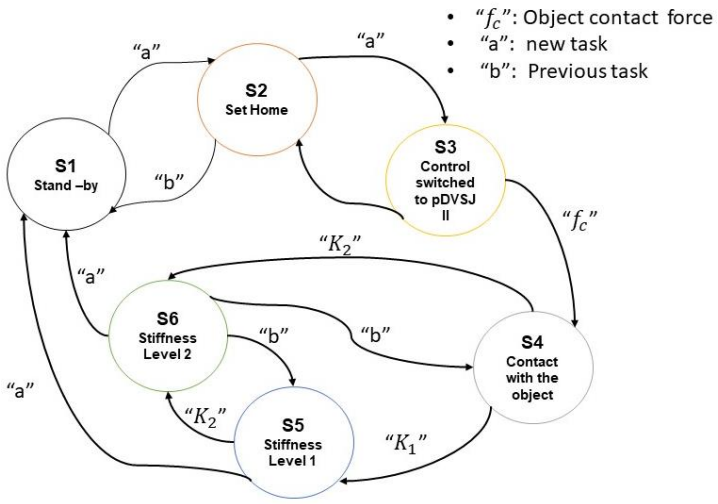

Figure. 21: The implementation of finite state machine (FSM) to perform the experimental tasks.

5.4. Results

The experimental results are detailed in Figures 22, 23 and 24. Fig. 22 shows the angular position of the pDVSJ-II device's end effector used to control the position of the end

effector of the Baxter manipulator in the vertical direction (see, Fig 23). The pDVSJ-II device's end effector position (Fig. 22) started at 25 degrees from the device's origin, where the spring started to coil and store energy. The user kept pushing towards 3 degrees. When the energy stored in the spring was released, the end-effector was pushed back to 25 degrees. Since the slave robot was controlled in the position mode, the same penetration distance was provided for both soft and rigid objects (Fig. 23) to measure the difference in the resultant force (plotted in Fig. 24). As expected, less force was found in the case of the soft object as compared to the stiffer object. The negative values of the force represent compression force. Using the information regarding the force and penetration distance, the resultant stiffness of the object was estimated using the simple relationship (k=$\Delta f/\Delta x$). The corresponding stiffness level was activated through the haptic interface. Moreover, the participants were asked about their satisfaction regarding the intuitiveness and ease of using the device for palpation application. The detailed results of this qualitative test is illustrated in Table 8. The results indicate that satisfaction was on average 3.83 out of 5 (0 reflects completely unsatisfied, and 5 reflects completely satisfied).

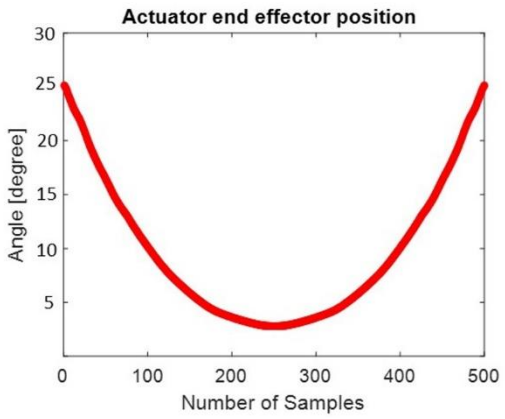

Figure 22. The rotation of our device's (pDVSJ-II) end effector to move the slave robot

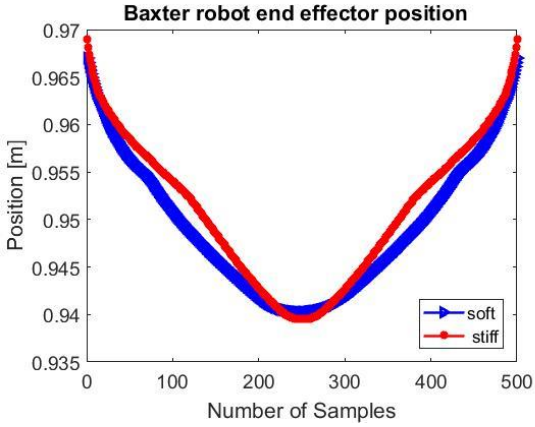

Figure. 23: Position of the Baxter robot end effector in case of both soft and relatively stiff objects.

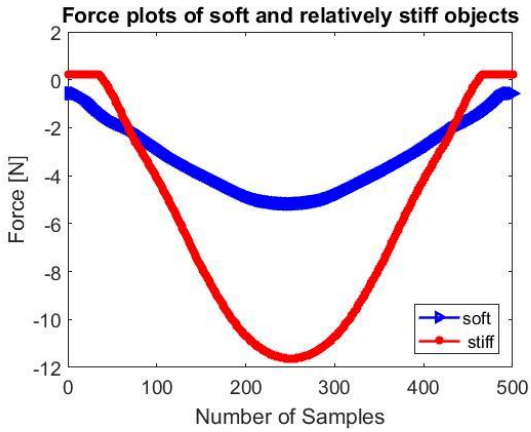

Figure .24: The force plots of the soft (blue) and relatively stiff (red)

Table 8: Qualitative Test Results

Questionnaire factors (out of 5; 0 reflects completely unsatisfied, and 5 reflects completely satisfied)	Subject 1	Subject 2	Subject 3	Average
Ease of use	4.5	5	5	4.83
Ease of learning	4	4.5	5	4.5
Satisfaction	3.5	4	4	3.83

6. DISCUSSION

The method of altering the stiffness in pDVSJ-II is achieved by instantaneously changing the number of involved elastic elements. The design allows for three discrete

levels of stiffness (zero, low, and high) with unobstructed rotation in the zero stiffness case applying simple, cost-effective, easily manufactured, light-weighted components, and low energy consumption. Altering the number of involved elastic elements has been previously introduced in the Series-Parallel Elastic Actuator (SPEA) applications. In the iSEPA actuator [47], the springs are connected to the output link from one side and to an intermittent mechanism on the other side. Such mechanism converts a continuous (rotational) input into two consecutive phases, yielding a succession of springs' involvement by altering the output torque of the actuator. MACCEPA-Based SPEA is another example of SPEA [48], where the springs are recruited through a cylindrical cam mechanism. These actuators can achieve more discrete levels of stiffness as compared to the pDVSJ-II as they include more springs in their design. On the other hand, the aforementioned mechanisms require an actuator to engage and disengage the elastic element, while in the pDVSJ-II, the disengagement process is passively achieved by moving the cord to the opposite side of the engagement side.

Further examples of variable stiffness mechanisms that were dedicated for passive haptic interfaces are illustrated in [25, 28, 36]. In [25], a grounded passive device for real time stiffness display was introduced. This device is capable of rendering a large range of stiffness levels but lacks the capability of rendering the zero level stiffness. In [36], a variable stiffness robotic probe for soft tissue palpation is presented. The design incorporates a Variable Lever Mechanism (VLM). This type of mechanisms would provide a continuous limited range of stiffness that can fit for a specific application, but with the proposed scheme, the range of stiffness does not include the zero stiffness level. In pVSJ

[28], also a large range of stiffness levels can be achieved (including the zero stiffness) through VLM, but it suffers from the relatively slow rate in changing these levels. Furthermore, the energy consumption in pVSJ is higher as compared to the pDVSJ-II since the stiffness in the pVSJ is dependent on the joint's position which requires the motor to stay on to maintain the same stiffness level. The pDVSJ-II, on the other hand, uses the ON-time for the linear solenoid in order to engage the cam-cleat which in turn creates and maintains the grounding point.

7. LIMITATIONS

pDVSJ-II falls under the category of passive haptic interfaces. Therefore, pDVSJ-II inherits the limitations of all passive haptic interfaces in their inability to generate a force that will change the direction of motion of the user's hand. This fact prevents passive haptic interfaces to be used in several applications like bilateral teleoperation with obstacle avoidance through artificial force fields [49].

The main purpose of pDVSJ-II is to fully simulate the interaction of elastic elements without sacrificing the natural passivity of its system. Thus, the applications where pDVSJ-II is used is limited to exploration and remote object stiffness rendering. As the system does not include controllable energy dissipative elements (i.e brakes), the system is incapable to control its damping coefficients preventing it from being used in haptic applications where motion redirecting is required (i.e. path following [50]).

As pDVSJ-II is still at the proof-of-concept level, the current version of the CGUs are quite bulky and limits the number of stiffness levels rendered by the device. Thus, in future, more compact version of CGU should be presented to enable more levels of stiffness to be rendered. The CGUs are unidirectional self-locking mechanisms with passive unlocking if a change in the cord's direction occurs. From this feature, pDVSJ-II can be equipped with a kinesthetic haptic glove to perform in applications like remote objects stiffness rendering and remote environment exploration (see figure 25). In such application, stiffness will only change when the users move their hand like they're compressing an object in their hands to check its stiffness. Thus, the CGUs will lock when the user compresses (squeezing) the object in their hand, and will unlock when the object is released.

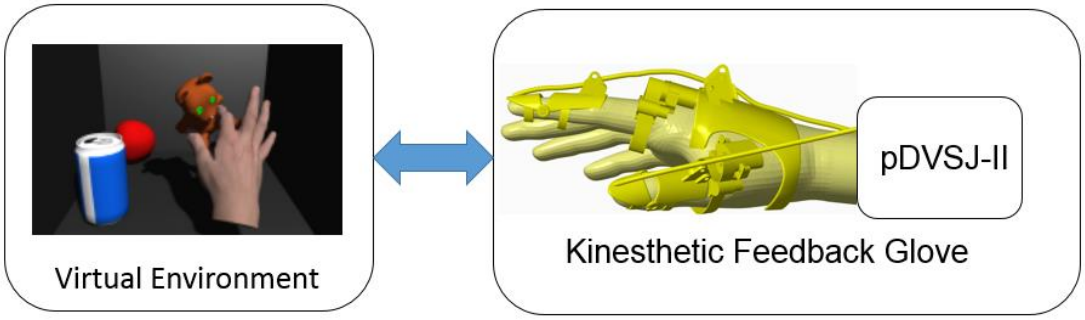

Figure 25: Suggested application for pDVSJ-II for remote exploration mission specifically for remote elements stiffness rendering.

As explained in section 2.3 the locking and the unlocking features of the CGUs would allow stiffness to be altered from low stiffness levels to higher levels of stiffness without the

need of unlocking the low-level CGUs. Applying the system illustrated in fig. 25, this feature will serve in stiffness rendering in exploration mission where the user usually compresses the material to check its stiffness. Stiffness in material compression usually behaves in a non-decreasing behavior [38]. Thus, pDVSJ-II is limited to remote exploration mission where the user would compress the remote object to check its stiffness.

8. CONCLUSIONS & FUTURE WORK

A novel passive Discreet Variable Stiffness Joint (pDVSJ-II) was introduced in this paper and the concept of using the joint for force reflection in haptics was explored. The mechanical design, physical model and system characterization of the joint were presented in detail. The joint's stiffness can be altered discretely through selecting the involved springs and the effective length of the High Stiffness Cord (HSC). The methodology used to realize the concept is novel to the best knowledge of the investigators. Altering the stiffness is achieved through activating one of the Cord Grounding Units, responsible for clutching the cord's motion, hence creating a new grounding point and limiting the effective length and involving corresponding springs.

A comprehensive study of the behavior elastic elements (Springs & High Stiffness Cord) was conducted and the stiffness properties of each element was applied to model the joint stiffness. Pretension was applied to ensure that pDVSJ-II operates only in the linear region of the elastic elements to reduce the model's complexity. The physical model was presented and validated through experimental results, which demonstrated that the joint is capable of altering the two levels of stiffness at each individual joint position. Furthermore, the novel design results in minimization of the energy-consumption, due

the self-locking feature allowing the Cord Grounding Unit to require short ON-Time for the linear actuator.

Human psychophysiological experiments were used to validate pDVSJ-II as an effective passive haptic device. Two psychophysiological tasks, based on literature, were conducted on 20 participants. The relative cognitive task aimed to measure the participants' ability to differentiate between different levels of stiffness simulated on the haptic device stylus. While the absolute cognitive task aimed to measure the participants' ability to relate of the stiffness simulated on the haptic device simultaneously with the calibrated value of stiffness. The results demonstrated good relative accuracy of the potential of pDVSJ-II to be used as a haptic device for simulating different levels of stiffness.

To further evaluate the capabilities of pDVSJ-II as a passive-haptic interface, an experimental setup was realized for remote medical application (diagnostic palpation using touch). The experimental scenario consisted of a remote manipulator (Baxter Robot) teleoperated by the pDVSJ-II, where the manipulator performed the remote palpation task feeding back the level of stiffness of the touched object through pDVSJ-II to the operator. Three participants performed the experiment successfully demonstrating system's capability, and intuitiveness to be used in such applications.

For future research, the authors intend to use elastic materials in order to produce an elastic cord with suitable performance specifications for the current application. This would lead the development of a more compact version of the CGU with optimized performance. Hence, more stiffness levels can be realized by adding more CGUs resulting

in a better representation of stiffness mapping. Finally, the authors recommend conducting an experiment similar to [42, 51] to evaluate and confirm the values of JND in stiffness levels. Such an experiment would help to fine tune the selection of the stiffness levels rendered by pDVSJ-II.

ACKNOWLEDGMENT

The authors would like to thank Dr. Nader Darwich, Chief of Orthopedics, and the Ethics Committee at HealthPoint Hospital for approving and facilitating the psychophysiological human experiments. The authors would also like to thank Mr. Jaideep Thattamparambil for helping in the fabrication process

REFERENCES

[1] Hayward, V., Astley, O., Cruz-Hernandez, M., Grant, D., and Robles-De-La-Torre, G., 2004, “Haptic interfaces and devices.” Sensor Review, 24(1), pp. 16–29. https://doi.org/10.1108/02602280410515770

[2] Lee, S., Sukhatme, G. S., Kim, G. J. and Park, C. M., 2002, "Haptic control of a mobile robot: a user study." IEEE/RSJ International Conference on Intelligent Robots and Systems, Lausanne, Switzerland, Sep 30 – Oct 4, pp. 2867-2874. doi: 10.1109/IRDS.2002.1041705

[3] Cho, S. K., Jin, H. Z., Lee, J. M., and Yao, B., 2010, "Teleoperation of a Mobile Robot Using a Force-Reflection Joystick With Sensing Mechanism of Rotating Magnetic Field." IEEE/ASME Transactions on Mechatronics, 15(1), pp. 17-26. doi: 10.1109/TMECH.2009.2013848

[4] Crespo, M., and Reinkensmeyer, DJ., 2008, “Haptic guidance can enhance motor learning of a steering task.” Journal of Motor Behavior, 40(6), pp. 545–556. DOI: 10.3200/JMBR.40.6.545-557.

[5] Chen, X. and Agrawal, S. K., 2013, "Assisting Versus Repelling Force-Feedback for Learning of a Line Following Task in a Wheelchair." IEEE Transactions on Neural Systems and Rehabilitation Engineering, 21(6), pp. 959-968. doi: 10.1109/TNSRE.2013.2245917

[6] Coles, T. R., Meglan, D., and John, N. W., 2011, "The Role of Haptics in Medical Training Simulators: A Survey of the State of the Art." IEEE Transactions on Haptics, 4(1), pp. 51-66. doi: 10.1109/TOH.2010.19.

[7] Ferre, M., Galiana, I., Wirz, R., and Tuttle, N., 2011, "Haptic Device for Capturing and Simulating Hand Manipulation Rehabilitation." IEEE/ASME Transactions on Mechatronics, 16(5), pp. 808-815. doi: 10.1109/TMECH.2011.2159807

[8] Gosselin, F., Bidard, C., and Brisset, J., 2005, "Design of a High Fidelity Haptic Device for Telesurgery." Proceedings of the 2005 IEEE International Conference on Robotics and Automation, Barcelona, Spain, April 18-22, pp. 205-210. doi: 10.1109/ROBOT.2005.1570120

[9] Wang, X., and Liu, P. X., 2006, "Improvement of haptic feedback fidelity for telesurgical applications." Electronics Letters, 42(6), pp. 327-329. doi: 10.1049/el:20064042

[10] Ni, Z., Bolopion, A., Agnus, J., Benosman, R., and Regnier, S., 2012 "Asynchronous Event-Based Visual Shape Tracking for Stable Haptic Feedback in Microrobotics." IEEE Transactions on Robotics, 28(5), pp. 1081-1089. doi: 10.1109/TRO.2012.2198930

[11] Bolopion, A., and Régnier, S., 2013, "A Review of Haptic Feedback Teleoperation Systems for Micromanipulation and Microassembly." in IEEE Transactions on Automation Science and Engineering, 10(3), pp. 496-502. doi: 10.1109/TASE.2013.2245122

[12] Salisbury, J. K., and Srinivasan, M., 1996, “The proceedings of the First Phantom Users Group Workshop”, Report No. AITR-1596, Massachusetts Institute of Technology, Massachusetts, USA. doi: http://hdl.handle.net/1721.1/6769

[13] Gupta, A., and O'Malley, M. K., 2006 "Design of a haptic arm exoskeleton for training and rehabilitation." IEEE/ASME Transactions on Mechatronics, 11(3), pp. 280-289. doi: 10.1109/TMECH.2006.875558

[14] Turner, M., Gomez, D., Tremblay, M., and Cutkosky, M. R., 1998, “Preliminary tests of an arm-grounded haptic feedback device in telemanipulation.” Symposium, Haptic interfaces for virtual environment and teleoperator systems, Anaheim, CA, pp.145-150. URL: http://citeseerx.ist.psu.edu/viewdoc/download?doi=10.1.1.329.1781&rep=rep1&type=pdf

[15] MA, Z., and Ben-Tzvi, P., 2015, "RML Glove—An Exoskeleton Glove Mechanism With Haptics Feedback." IEEE/ASME Transactions on Mechatronics, 20(2), pp. 641-652. doi: 10.1109/TMECH.2014.2305842

[16] Swanson, D., 2003, ”Implementation of Arbitrary Path Constraints using Dissipative Passive Haptic Displays.” PhD thesis, School of Mechanical Engineering, Georgia Institute of Technology, Atlanta, GA. URL: http://imdl.gatech.edu/davin/research/IRB_protocol_v2.pdf

[17] Rossa, C., Lozada, J., and Micaelli, A., 2014, "Design and Control of a Dual Unidirectional Brake Hybrid Actuation System for Haptic Devices." IEEE Transactions on Haptics, 7(4), pp. 442-453. doi: 10.1109/TOH.2014.2346501

[18] Nam, Y.J., and Park, M.K., 2007, “"A hybrid haptic device for wide-ranged force reflection and improved transparency." 2007 International Conference on Control, Automation and Systems, Seoul, South Korea, October 17-20, pp. 1015-1020. doi: 10.1109/ICCAS.2007.4407046

[19] Book, W., Charles, R., Davis, H. T., and Gomes, M., 1996, “The concept and implementation of a passive trajectory enhancing robot." Proceedings of the ASME Dynamic Systems and Control Division, Atlanta, GA, pp. 633-638. URL: http://hdl.handle.net/1853/39068

[20] Sakaguchi M., and Furusho, J., 1999, "Development of 2 DOF force display system using ER actuators," 1999 IEEE/ASME International Conference on Advanced Intelligent Mechatronics (Cat. No.99TH8399), Atlanta, GA, USA, pp. 707-712. doi: 10.1109/AIM.1999.803254

[21] Tenzer, Y., Davies, B. L., and Rodriguez y Baena, F., 2010,” Programmable differential brake for passive haptics.” Robotics and Autonomous Systems, 58(3), pp. 249-255. Doi: https://doi.org/10.1016/j.robot.2009.08.003

[22] Gosline, A. H. C., and Hayward, V., 2008 "Eddy Current Brakes for Haptic Interfaces: Design, Identification, and Control." IEEE/ASME Transactions on Mechatronics, 13(6), pp. 669-677. doi: 10.1109/TMECH.2008.2004623

[23] Achibet, M., Girard, A., Talvas, A. , Marchal M., and Lécuyer, A., 2015 "Elastic-Arm: Human-scale passive haptic feedback for augmenting interaction and perception in virtual environments," 2015 IEEE Virtual Reality (VR), Arles, France, March 23-27, pp. 63-68. doi: 10.1109/VR.2015.7223325

[24] Bianchi, M., Scilingo, E. P. , Serio, A., and Bicchi, A., 2009, "A new softness display based on bi-elastic fabric," World Haptics 2009 - Third Joint EuroHaptics conference and Symposium on Haptic Interfaces for Virtual Environment and Teleoperator Systems, Salt Lake City, UT, USA, March 18-20, pp. 382-383. doi: 10.1109/WHC.2009.4810905

[25] Song, A., Morris D., Colgate, J. E., and Peshkin, M. A., 2005, "Real time stiffness display interface device for perception of virtual soft object." 2005 IEEE/RSJ International Conference on Intelligent Robots and Systems, Edmonton, Alberta, August 2-6, pp. 139-143. doi: 10.1109/IROS.2005.1545131

[26] Basafa, E., Sheikholeslami, M., Mirbagheri, A., Farahmand, F., and Vossoughi, G.R., 2009, "Design and implementation of series elastic actuators for a haptic laparoscopic device." 2009 Annual International Conference of the IEEE Engineering in Medicine and Biology Society, Minneapolis, MN, Sep. 2-6, pp. 6054-6057. doi: 10.1109/IEMBS.2009.5332616

[27] Gan, D. Tsagarakis, NG., Dai, JS., Caldwell, DG., and Seneviratne, L., 2012, “Stiffness Design for a Spatial Three Degrees of Freedom Serial Compliant Manipulator Based

on Impact Configuration Decomposition." ASME. J. Mechanisms Robotics, 5(1), pp. 011002-011002-10. doi:10.1115/1.4007492.

[28] Awad, M. I., Gan, D., Cempini, M., Cortese, M., Vitiello, N., Dias, J., Dario, P., and Seneviratne, L., 2016, "Modeling, design & characterization of a novel Passive Variable Stiffness Joint (pVSJ)." 2016 IEEE/RSJ International Conference on Intelligent Robots and Systems (IROS), Daejeon, South Korea, Oct. 9-14, pp. 323-329. doi: 10.1109/IROS.2016.7759074.

[29] Tonietti, G., Schiavi, R., and Bicchi, A., 2005, "Design and Control of a Variable Stiffness Actuator for Safe and Fast Physical Human/Robot Interaction." Proceedings of the 2005 IEEE International Conference on Robotics and Automation, Barcelona, Spain, April 18-22, pp. 526-531. doi: 10.1109/ROBOT.2005.1570172

[30] Diller , S., Majidi, C., and Collins, S. H., 2016, "A lightweight, low-power electroadhesive clutch and spring for exoskeleton actuation." 2016 IEEE International Conference on Robotics and Automation (ICRA): Stockholm, Sweeden, May 16-21, pp. 682-689. doi: 10.1109/ICRA.2016.7487194

[31] Hurst , J. W., Chestnutt, J. E., and Rizzi, A. A., 2010, "The Actuator With Mechanically Adjustable Series Compliance." IEEE Transactions on Robotics, 26(4), pp. 597-606. doi: 10.1109/TRO.2010.2052398.

[32] Zhou, X., Jun, S., and Krovi, V., 2015, "A Cable Based Active Variable Stiffness Module With Decoupled Tension." ASME. J. Mechanisms and Robotics, 7(1), 011005-011005-5. doi:10.1115/1.4029308.

[33] Jafari, A., Tsagarakis, N. G., Vanderborght, B., and Caldwell, D. G., 2010, "A novel actuator with adjustable stiffness (AwAS)." 2010 IEEE/RSJ International Conference on Intelligent Robots and Systems, Taipei, Taiwan, Oct. 18-22, pp. 4201-4206. doi: 10.1109/IROS.2010.5648902

[34] Jafari, A., Tsagarakis, N. G., and Caldwell, D. G., 2011, "AwAS-II: A new Actuator with Adjustable Stiffness based on the novel principle of adaptable pivot point and variable lever ratio." 2011 IEEE International Conference on Robotics and Automation, Shanghai, China, May 9-13, pp. 4638-4643. doi: 10.1109/ICRA.2011.597999

[35] Tsagarakis, N.G., Sardellitti, I., and Caldwell, D. G., 2011, "A new variable stiffness actuator (CompAct-VSA): Design and modelling." 2011 IEEE/RSJ International

Conference on Intelligent Robots and Systems, San Francisco, CA, Sep. 25-30, pp. 378-383. doi: 10.1109/IROS.2011.6095006

[36] Herzig, N., Maiolino, P., Iida, F. and Nanayakkara, T., 2018, "A Variable Stiffness Robotic Probe for Soft Tissue Palpation," IEEE Robotics and Automation Letters, 3(2), pp. 1168-1175. doi: 10.1109/LRA.2018.2793961

[37] Awad, M. I., Gan, D., Az-zu'bi, A., Thattamparambil, J., Stefanini, C., Dias, J., and Seneviratne, L., 2016, "Novel passive Discrete Variable Stiffness Joint (pDVSJ): Modeling, design, and characterization." 2016 IEEE International Conference on Robotics and Biomimetics (ROBIO), Qingdao, China, Dec 3-7, pp. 1808-1813. doi: 10.1109/ROBIO.2016.7866591

[38] Dzidek, B. M., Adams, M. J., Andrews, J. W., Zhang, Z., and Johnson, S. A., 2017, "Contact mechanics of the human finger pad under compressive loads." Journal of The Royal Society Interface, 14(127), pp. 1 -13. doi: 10.1098/rsif.2016.0935

[39] Treloar, L., and Ronald, G., 2005, "The physics of rubber elasticity." Oxford University Press, Oxford, UK.

[40] Love, A. E., 1920, "A treatise on the mathematical theory of elasticity" Dover Publications, NY, USA

[41] Bianchi, M., Battaglia, E., Poggiani, M., Ciotti, S., and Bicchi, A., 2016, "A Wearable Fabric-based display for haptic multi-cue delivery," 2016 IEEE Haptics Symposium (HAPTICS), Philadelphia, PA, April 8-11, pp. 277-283. doi: 10.1109/HAPTICS.2016.7463190

[42] Koçak, U., Palmerius, K.L., Forsell, C., Ynnerman, A., and Cooper, M., 2011, "Analysis of the JND of Stiffness in Three Modes of Comparison." International Workshop on Haptic and Audio Interaction Design, Berlin, Heidelberg, pp.22-31. DOI: https://doi.org/10.1007/978-3-642-22950-3_3

[43] Amiguet, J., Sessa, S., Bleuler, H., and Takanishi, A., 2015, "Design of a wearable device for low frequency haptic stimulation." 2015 IEEE International Conference on Robotics and Biomimetics (ROBIO), Zhuhai, China, Dec. 6-9, pp. 297-302. doi: 10.1109/ROBIO.2015.7418783

[44] Konstantinova, J., Cotugno, G., Dasgupta, P., Althoefer, K., and Nanayakkara, T., 2018, "Correction: Palpation force modulation strategies to identify hard regions in soft tissue organs." PloS one, 13(1), pp. 1-24. doi: doi.org/10.1371/journal.pone.0192259

[45] Goodrich, M. A., and Schultz, A. C., 2008, "Human–robot interaction: a survey." Foundations and Trends® in Human–Computer Interaction, 1(3), pp. 203-275. Doi: 10.1561/1100000005

[46] Quigley, M., Conley, K., Gerkey, B. P., Faust, J., Foote, T., Leibs, J., Wheeler, R., and Ng, Andrew Y., 2009, "ROS: an open-source Robot Operating System." ICRA workshop on open source software, 3(3.2), pp. 1-5 URL: http://www.willowgarage.com/sites/default/files/icraoss09-ROS.pdf

[47] Mathijssen, G., Lefeber, D., and Vanderborght, B., 2015, "Variable Recruitment of Parallel Elastic Elements: Series–Parallel Elastic Actuators (SPEA) With Dephased Mutilated Gears." IEEE/ASME Transactions on Mechatronics, 20(2), pp. 594-602. doi: 10.1109/TMECH.2014.230712

[48] Mathijssen, G., Furnemont, R., Beckers, S., Verstranten, T., Lefeber, D., and Vanderborght, B., 2015. "Cylindrical cam mechanism for unlimited subsequent spring recruitment in Series-Parallel Elastic Actuators." 2015 IEEE International Conference on Robotics and Automation (ICRA), Seattle, WA, May 25-30, pp. 857-862. doi: 10.1109/ICRA.2015.7139278

[49] Islam, S., Gan, D., Ashour, R., Dario, P., Dias, J., and Seneviratne, L., 2017, "Haptics and virtual reality based bilateral telemanipulation of miniature aerial vehicle over open communication network." 2017 18th International Conference on Advanced Robotics (ICAR), Hong Kong, July 10-12, pp. 334-339. doi: 10.1109/ICAR.2017.8023629

[50] Wannasuphoprasit, W., Gillespie, R.B., Colgate, J.E., and Peshkin, M.A., 1997, "Cobot control." Proceedings of International Conference on Robotics and Automation, Albuquerque, NM, USA, April 20-25, pp. 3571-3576. doi: 10.1109/ROBOT.1997.606888

[51] Karadogan, E., Williams, RL 2nd., Howell, JN., and Conaster, RR Jr., 2010, "A stiffness discrimination experiment including analysis of palpation forces and velocities." Simulation in Healthcare, 5(5), pp 279-288. doi: 10.1097/SIH.0b013e3181e9e783

Figure Captions List

Fig. 1 pDVSJ mounted on an elbow exoskeleton [37]

Fig. 16 The bode plot of the system for both levels of stiffness (High: red, Low: blue). The bandwidth for the system in high stiffness and low stiffness are 8.52 Hz, 5.88 Hz, respectively

Fig. 17 Stiffness Mimic Devices with Calibrated Springs

Fig. 18 Participant performing the Absolute Cognitive Task

Fig. 19 The experimental set up: The Baxter manipulator having the tracking markers at its end effector to register the vertical motion. The haptic interface (pDVSJ-II) has tracking marker at its end effector. The motion of both robot and pDVSJ-II end effector are recorded through Optitrack system. The ATI Delta force sensor is placed under the object to measure the applied force. Arduino Uno along with the 24V relays is used to activate/deactivate the solenoid to alter the stiffness of the device

Fig. 20 Block Diagram of experimental setup. The Optitrack system to record the motion at both master and slave side i.e. the position of end effector's of robot and pDVSJ-II device and communicate with the computer through ROS. On the slave side, the Baxter Robot, ATI Delta along with its NetBox controller are connected with the computer and also use the ROS as communication interface. On master side, the arduino UNO is connected with computer through serial communication which in turns control the relays to activate/deactivate the solenoids to change the stiffness of pDVSJ-II accordingly.

Fig. 21 The implementation of finite state machine (FSM) to perform the experimental tasks

Fig. 22 The rotation of our device's (pDVSJ-II) end effector to move the slave robot

Fig. 23 Position of the Baxter robot end effector in case of both soft and relatively stiff objects

Fig. 24 The force plots of the soft (blue) and relatively stiff (red)

Fig. 25 Suggested application for pDVSJ-II for remote exploration mission specifically for remote elements stiffness rendering.

Table Caption List

Table 1 Cam-cleat profile constants

Table 2 pDVSJ-II Design Parameters & Specifications

Table 3 System's Power and Physical Specifications

Table 4 Dynamics System Coefficients for pDVSJ-II

Table 5 Springs parameters for the Stiffness Mimic Devices

Table 6 Confusion Matrix of Relative Cognitive Task

Table 7 Confusion Matrix of Absolute Cognitive Task

Table 8 Qualitative Test Results